PHYSICAL REVIEW A **79**, 051604(R) (2009)

Quantum phase diagram of fermion mixtures with population imbalance in one-dimensional optical lattices

B. Wang, Han-Dong Chen, and S. Das Sarma
Department of Physics, Condensed Matter Theory Center and Center for Nanophysics and Advanced Materials, University of Maryland, College Park, Maryland 20742-4111, USA

(Received 30 January 2009; revised manuscript received 10 March 2009; published 14 May 2009)

With a recently developed time-evolving block decimation algorithm, we numerically study the ground-state quantum phase diagram of Fermi mixtures with attractive interspecies interactions loaded in one-dimensional optical lattices. For our study, we adopt a general asymmetric Hubbard model with species-dependent tunneling rates to incorporate the possibility of mass imbalance in the mixtures. We find clear signatures for the existence of a Fulde-Ferrell-Larkin-Ovchinnikov (FFLO) phase in this model in the presence of population imbalance. Our simulation also reveals that in the presence of mass imbalance, the parameter space for FFLO states shrinks or even completely vanishes depending on the strength of the attractive interaction and the degree of mass imbalance.

DOI: 10.1103/PhysRevA.79.051604 PACS number(s): 67.85.−d, 03.75.Ss, 71.10.Fd

The pairing of fermions in multicomponent Fermi mixtures is of fundamental interest for a broad range of active research fields in most branches of modern physics, such as superconductivity in condensed-matter physics, novel states of matter in ultracold atom systems, neutron stars in astrophysics [1], as well as color superconductivity of quark matter in nuclear and elementary particle physics [2]. When the Fermi surfaces of the component species are mismatched due to unequal densities, possibilities open up for exotic pairing mechanisms such as the Fulde-Ferrell-Larkin-Ovchinnikov (FFLO) [3,4] and the breached pair (BP) states [5,6]. While these interesting states of matter remain experimentally elusive, controversies about their stability have been long standing. Recently, this subject has received renewed intense attention due to the atomic physics experimental studies on population-imbalanced ultracold fermions [7]. The advent of the techniques for precisely controlling and detecting ultracold atoms is making it possible to systematically study the FFLO and/or the BP states with exotic fermionic pairing, which has turned out to be impossible to do in conventional solid-state systems.

Inspired by the experimental achievements, over the past few years a large body of theoretical studies have been reported on the exotic pairing states in ultracold atomic fermion systems with population imbalance [8–11]. It has been found that both the FFLO [8] and the BP states [9] could exist in three-dimensional (3D) systems. Particularly, a consensus has developed that the stability region of the 3D FFLO states is very narrow especially at finite temperature, making it very difficult to observe experimentally. In contrast, due to the Fermi-surface nesting it could be much easier to observe the FFLO-type states in one-dimensional (1D) or quasi-1D systems [10,11]. In this work we present numerically calculated exact quantum phase diagrams for the population imbalanced 1D Fermi mixtures with unequal masses for the component species.

Fermi mixture systems with mass imbalance could be characterized by the asymmetric Hubbard model (AHM) with species-dependent tunneling rates. With equal spin populations, a phase diagram for the 1D AHM has been obtained with the renormalization-group technique [12], and possible spin segregation in this model with repulsive interactions has been investigated with bosonization and density-matrix renormalization-group (DMRG) techniques [13]. Nonetheless, it is not surprising that more attention has been given to the case with both mass and population imbalances, in which stabilities of FFLO and BP states in 3D systems have been extensively studied [14]. Very recently, a quantum Monte Carlo (QMC) study on finite-size Fermi mixtures in 1D optical lattices with imbalanced populations and masses has been reported [15], in which the evidence of 1D analog of FFLO-type states has been found. The QMC simulation also reveals that when the mass difference is large enough, instead of being an FFLO-type state, the ground state of the system will become an inhomogeneous "collapsed" state.

In this Rapid Communication, we report a time-evolving block decimation (TEBD) numerical study on Fermi mixtures with unequal masses and attractive on-site interaction in 1D optical lattices. Our study is complementary to the QMC simulation in Ref. [15], in that we obtain the phase diagrams for such Fermi mixture systems. Consistent with the QMC results, we find that FFLO states are the only possible class of polarized pairing states in such systems. As the mass imbalance increases, the parameter space for FFLO states shrinks and eventually vanishes completely. Since we study the homogeneous system in the thermodynamic limit, the inhomogeneous collapsed state does not show up here, in contrast to Ref. [15].

For our simulation, we adopt the asymmetric Hubbard Hamiltonian to model the Fermi mixtures in 1D optical lattices with unequal masses:

$$H = -\sum_{\langle i,j\rangle,\sigma} t_\sigma c_{\sigma i}^\dagger c_{\sigma j} + \sum_i U n_{\uparrow i} n_{\downarrow i} - \sum_i \mu(n_{\uparrow i} + n_{\downarrow i}) + \sum_i \delta\mu(n_{\downarrow i} - n_{\uparrow i}), \quad (1)$$

where $c_{\sigma i}$ ($\sigma = \uparrow$ or $\downarrow$) stands for the annihilation operator of σ fermion at site i, $n_{\sigma i}(=c_{\sigma i}^\dagger c_{\sigma i})$ represents the corresponding particle number operator, t_σ is the species-dependent tunneling rate (through out this Rapid Communication $t_\uparrow$ is set to be the unit of energy), U characterizes the on-site interspe-

cies interaction strength, and $\mu \pm \delta\mu$ gives the chemical potential of the $\uparrow/\downarrow$ fermion. In analogy with real spin systems, $\delta\mu$ will be referred as the effective magnetic field in the following although our system is spinless with the $\uparrow/\downarrow$ components corresponding to fermions with different masses. The unequal mass effects are incorporated in the species-dependent tunneling rates through

$$\frac{t_\downarrow}{t_\uparrow} = \frac{m_\uparrow}{m_\downarrow}. \tag{2}$$

We note that the asymmetric Hubbard model in Eq. (1) could also be realized in mixtures of same-species fermions prepared in two different internal states by engineering internal-state-dependent optical lattices [16].

To investigate the ground state properties of Hamiltonian (1), we use an infinite lattice version of the TEBD algorithm [17], which allows us to study the model in the thermodynamic limit. A source of the intrinsic numerical error for TEBD is due to the Trotter-Suzuki expansion (TSE) for the decomposition of time evolution operator. (In our simulation we have chosen the fourth-order symmetric TSE.) Furthermore, the convergence of the physical results with TEBD is mainly controlled by a cut-off parameter χ, which characterizes how well one preserves the bipartite entanglement of the system when truncating the Hilbert space. In this work, we choose $\chi=60$. The convergence has been checked to be good enough [within $\sim O(10^{-4})$ for real-space correlation functions] for our purpose by comparing with $\chi=80$ and 100 results.

To identify relevant (quasi)phases for our model, we calculate the real-space spin-spin (S_r^m), density-density (D_r), and pairing (P_r) correlations and their Fourier transforms $X_k = 1/\sqrt{M}\Sigma_{r=0}^{M} X_r \cos(kr)$, where $M+1$ is the number of sites involved in the transforms (for this work, we choose $M=100$) and X stands for S, D, and P correlations. The real-space correlation functions are defined as

$$S_r^m \equiv \langle \mathbf{s}_i^m \mathbf{s}_{i+r}^m \rangle - \langle \mathbf{s}_i^m \rangle \langle \mathbf{s}_{i+r}^m \rangle,$$

$$D_r \equiv \langle n_i n_{i+r} \rangle - \langle n_i \rangle \langle n_{i+r} \rangle,$$

$$P_r \equiv \langle c_{i\uparrow} c_{i\downarrow} c_{i+r\downarrow}^\dagger c_{i+r\uparrow}^\dagger \rangle, \tag{3}$$

where the spin operators associated with site i is given by $\mathbf{s}_i^m \equiv c_{i\alpha}^\dagger \sigma_{\alpha\beta}^m c_{i\beta}/2$, with α and $\beta = \downarrow, \uparrow$ and σ^m $(m=x,y,z)$ stands for the Pauli matrices. In addition, we also calculate $\langle c_{\sigma i}^\dagger c_{\sigma i+r} \rangle$ and its Fourier transform $\langle n_{\sigma,k} \rangle$, which gives the momentum distribution of the σ fermion.

In Fig. 1, we present the ground-state phase diagrams for Fermi mixtures based on Hamiltonian (1) at $U=-4$. In the shaded parameter regions around the centers of the diagrams, all the lattice sites are partially filled by both species of fermions and the effective magnetic field $\delta\mu$ is not strong enough to induce any population imbalance. In these regions, the ground states of the system have either charge-density wave (CDW) or singlet superfluid (SS) as the dominant quasi-long-range order depending on the filling factor. As the effective magnetic field increases, population imbalance is introduced and the system could be brought into the regions

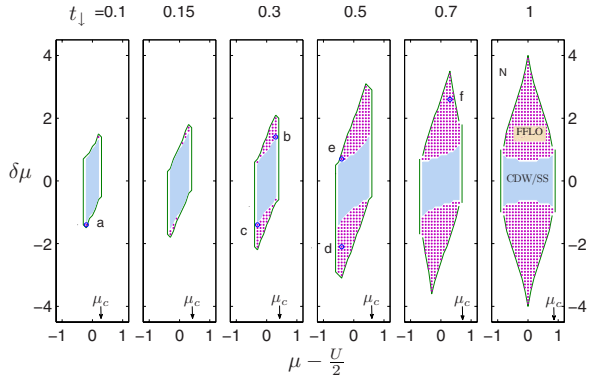

FIG. 1. (Color online) Effective magnetic field vs chemical potential ground-state phase diagrams for $U=-4$. From left to right, the six panels correspond to $t_\downarrow=0.1$, 0.15, 0.3, 0.5, 0.7, and 1, respectively. The ground states of the system in the regions filled with solid dots are found to be of the FFLO type. In the shaded regions around the center of each panel, the system has balanced population in its ground states. From $|\mu - U/2| = 0^+$ to μ_c, the dominant or subdominant quasi-long-range orders changes from CDW or SS to SS or CDW. In the remaining regions, at least one species of fermions satisfies $\langle n_{\sigma i} \rangle = 0$ or 1 and the system behaves as normal Fermi gas. The unit of energy is set to be $t_\uparrow$.

filled with solid dots as shown in Fig. 1. These regions are of central interest to us since within them the ground state of the system is found to be of the FFLO type. In the remaining regions of the diagrams, at least one type of fermions has zero or unity occupation number at all sites ($\langle n_{\sigma i} \rangle = 0$ or 1) and the system behaves as normal Fermi gas. The solid lines in Fig. 1 show the phase boundaries of the normal (N) states. We note that the normal states here could be further divided into different categories, i.e., vacuum state, fully occupied state, and fully polarized state, according to the occupation number and the degree of polarization. But as they are of limited interest, we do not distinguish them in this work.

By comparing the diagrams corresponding to different $t_\downarrow$, we can make the following observations. First, the parameter space supporting the FFLO state shrinks with the increase in the imbalance in t_σ or, equivalently, in the fermion masses. This can be understood by considering the bandwidth. A larger mass imbalance effectively leads to a narrower bandwidth ($\sim 4t_\downarrow^2/U$); hence when we tune μ or $\delta\mu$ it is easier for the system to fall into the $n_\downarrow = 0$ or 1 bands and become normal. A second observation is that the symmetry of the $t_\downarrow \neq 1$ diagrams is different from that in the $t_\downarrow = 1$ case. When $t_\downarrow \neq 1$, the diagrams are only symmetric about the center point $(\mu = U/2, \delta\mu = 0)$, reflecting the fact that the Hamiltonian is invariant under the particle-hole transformation combined with the inversion about $(\mu = U/2, \delta\mu = 0)$. In the $t_\downarrow = 1$ case, the diagram is symmetric about the two axes $\mu = U/2$ and $\delta\mu = 0$ since the Hamiltonian now possesses an extra symmetry, namely, the invariance under spin flip combined with the inversion about $(\mu = U/2, \delta\mu = 0)$.

We present in Fig. 2 the ground-state phase diagram for $U=-10$. One can see that the key features are the same as those in the $U=-4$ case. Namely, FFLO states are the only partially polarized superfluid states in the phase diagrams, and their parameter spaces shrink with an increase in mass

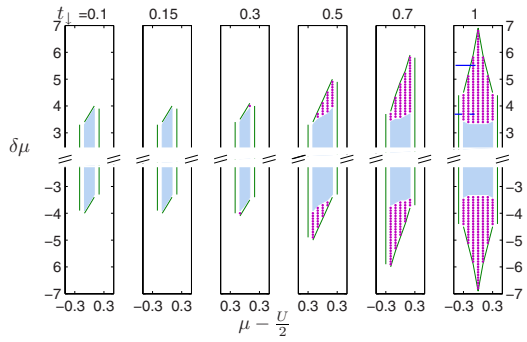

FIG. 2. (Color online) Effective magnetic field vs chemical potential ground-state phase diagrams for $U=-10$. From left to right, the six panels correspond to $t_\downarrow=0.1$, 0.15, 0.3, 0.5, 0.7, and 1, respectively. The ground states of the system in the regions filled with solid dots are FFLO-type states. In the shaded regions, the fermions of different species have equal population. In the remaining regions, the system behaves as normal Fermi gas. The unit of energy is set to be $t_\uparrow$.

imbalance. Furthermore, the shape and symmetry of the diagrams also resemble those in the $U=-4$ case. Nonetheless, there are noticeable differences. With a stronger on-site attraction, it is harder to break the pairs. Hence we have higher critical fields $\delta\mu_c$ in the $U=-10$ case. Besides, the effects of unequal masses become more dramatic when the on-site interaction is stronger. For example, in contrast to the $U=-4$ case, when $U=-10$ and $t_\downarrow=0.3$ one can barely find the FFLO phase and at $t_\downarrow=0.15$ the parameter space for FFLO completely disappears for $U=-10$.

It is also of interest to compare our results with previous studies on Fermi mixtures in harmonic traps with population imbalance and *equal* mass [11]. When $t_\downarrow=1$, Hamiltonian (1) reduces to the conventional Hubbard model. By fixing $\delta\mu$ and reducing μ in the dilute case (at most half-filled at the trap center), one can mimic the scenario of moving from the center to the edge in a harmonic trap according to the local-density approximation (LDA). With finite polarization, at the trap center the system is in an FFLO-type state. At large $|\delta\mu|$, a phase separation between the FFLO and fully polarized normal states is found (see the solid horizontal line in Fig. 2). In the case with small population imbalance, the Fermi mixture could be found in FFLO across the entire trap (see the dashed horizontal line in Fig. 2). Therefore our results are in qualitative agreement with previous studies.

In Fig. 3, we show the pairing correlation functions and particle number distributions in the momentum space for six sample data points with various $\{t_\downarrow,\mu,\delta\mu\}$ in the FFLO regimes of Fig. 1. An FFLO pair is known to have nonzero center-of-mass momentum, and as its signature, the pairing correlation function P_k shows a peak at the nonzero momentum $|k_{\uparrow F}-k_{\downarrow F}|$, with $k_{\sigma F}\equiv\langle n_{\sigma i}\rangle\pi$ as the Fermi momentum of noninteracting free fermions. From the solid curves in Fig. 3, we can clearly see the peaks of P_k at nonzero momenta $k_p=|k_{\uparrow F}-k_{\downarrow F}|$, indicating the presence of the FFLO pairing. One can also see that the particle number distribution functions $N_{\uparrow k}$ and $N_{\downarrow k}$ drop sharply at $k_{\uparrow F}$ and $k_{\downarrow F}$, respectively. Another noteworthy point is that the momentum distribution function for the "heavier" species ($\downarrow$ fermion) in an FFLO state clearly exhibits a dip at momentum $2k_{\uparrow F}-k_{\downarrow F}$.

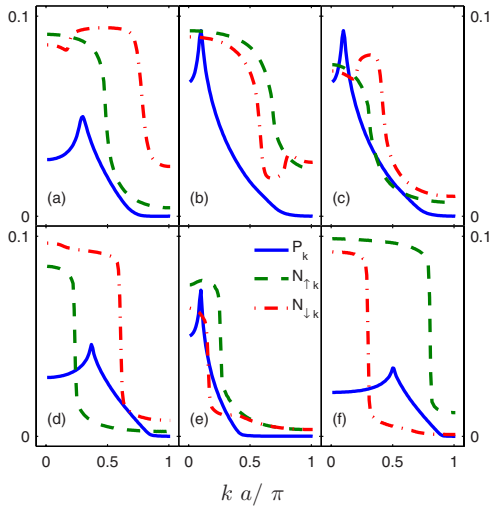

FIG. 3. (Color online) Fourier transforms of the pairing correlation functions (P_k) and particle number distributions ($N_{\uparrow k}$ and $N_{\downarrow k}$) for the partially polarized asymmetric Hubbard model at $U=-4$. P_k, $N_{\uparrow k}$, and $N_{\downarrow k}$ are depicted by the solid, dashed, and dash-dotted curves, respectively. Other parameters $\{t_\downarrow,\mu,\delta\mu\}$: (a) $\{0.1,-2.2,-1.4\}$; (b) $\{0.3,-1.7,1.4\}$; (c) $\{0.3,-2.3,-1.4\}$; (d) $\{0.5,-2.4,-2.1\}$; (e) $\{0.5,-2.4,0.7\}$; and (f) $\{0.7,-1.7,2.6\}$. The unit of energy is set to be $t_\uparrow$. Note that the data points corresponding to these parameter sets are marked in Fig. 1.

Considering the potential interests in studying the mixtures of ^{6}Li and ^{40}K experimentally [18], we also present the momentum space pairing (P_k) and density (D_k) correlations for the asymmetric Hubbard model at $U=-4$ and $t_\downarrow/t_\uparrow=0.15$. The two upper panels of Fig. 4 show the pairing and density correlations in the case with population imbalance, while the lower panels show the case with equal populations. From the visibility and height of the peaks in the correlation functions, one can tell which kind order is more dominant. First, we look into the case with equal popula-

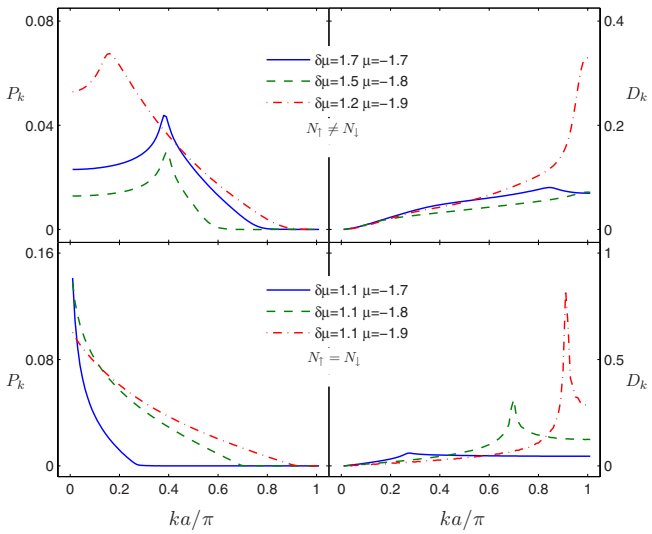

FIG. 4. (Color online) Momentum space pairing and density correlation functions for the asymmetric Hubbard model at $U=-4t_\uparrow$ and $t_\downarrow/t_\uparrow=0.15$, which is exactly the mass ratio between ^{6}Li and ^{40}K.

tions. When the filling factor slightly deviates from half filling, charge-density wave is the dominant quasi-long-range order. As an example, for $\delta\mu=1.1$ and $\mu=-1.9$, we have $\langle n_i\rangle=2k_{\uparrow F}=2k_{\downarrow F}\sim 1.09$. One can observe a sharp peak for D_k locating at $k\sim 0.9\pi(=2\pi-2k_{\sigma F})$, while P_k shows a much broader and lower peak at $k=0$ indicating that CDW is more dominant than SS. When the filling factor is further away from half filling, the singlet superfluid order becomes more dominant. (The peak of D_k moves toward $k=0$ with decreasing visibility and height, while the peak of P_k remains at $k=0$ and becomes sharper.) Next, we examine the case with population imbalance. From the upper left panel of Fig. 4, we can see that P_k has maxima at nonzero momenta, which are verified to be directly given by the difference in particle number density, signaling the presence of FFLO pairing. The results in Fig. 4 indicate that in order to observe the FFLO state in mixtures of spinless ^{6}Li and ^{40}K, one should keep the density of ^{40}K well away from half filling and avoid large interspecies interactions. It is well known that if weak tunneling between arrays of 1D tubes is allowed (quasi-1D), the leading quasi-long-range order in a 1D system could be stabilized and become real long-range order. Also the Fermi-surface nesting is greatly enhanced in lower dimensions as compared with the 3D case. So it could be advantageous to carry out the experiments in the quasi-1D setup in order to observe FFLO states. Finally, The experimental detection of FFLO states is also an important issue. One of the well-established probes for the phase correlation is the dynamical projection of the fermion pairs into condensate of deeply bound molecules followed by the measurement on the pair momentum distribution of the condensate with time-of-flight imaging. The signature of an FFLO state would be a peak at finite momentum set by the excess fermion density $q=|n_\uparrow-n_\downarrow|\pi$. In addition to the traditional time-of-flight imaging technique, schemes such as atom shot-noise correlation measurement [19] and Fourier sampling of time-of-flight images [20] have been proposed to probe the state of matter in ultracold Fermi gases. The noise correlation of the time-of-flight image $G_{\sigma\sigma'}(k,k')\equiv\langle n_{\sigma,k}n_{\sigma',k'}\rangle-\langle n_{\sigma,k}\rangle\langle n_{\sigma',k'}\rangle$ can detect the presence of FFLO states unambiguously by showing correlation at momenta satisfying $|k+k'|=q$.

In summary, we have presented the effective magnetic field ($\delta\mu$) vs chemical potential (μ) quantum phase diagrams for Fermi mixtures with unequal masses and attractive on-site interspecies interactions loaded in 1D optical lattices. We find that with mass and population imbalance the ground state of the system could be either an FFLO state or a normal state. With the increase in mass imbalance, the parameter space for the FFLO states shrinks. When the mass imbalance gets too large, the FFLO states are no longer stable.

We acknowledge helpful comments from A. Feiguin and W. V. Liu. This work was supported by ARO-DARPA.

[1] D. J. Dean and M. Hjorth-Jensen, Rev. Mod. Phys. **75**, 607 (2003); S. Reddy and G. Rupak, Phys. Rev. C **71**, 025201 (2005).

[2] M. Alford *et al.*, Phys. Rev. Lett. **84**, 598 (2000); M. Alford *et al.*, Phys. Rev. D **63**, 074016 (2001); I. Shovkovy *et al.*, Phys. Lett. B **564**, 205 (2003); R. Casalbuoni and G. Nardulli, Rev. Mod. Phys. **76**, 263 (2004); M. Alford *et al.*, *ibid.* **80**, 1455 (2008).

[3] P. Fulde and R. A. Ferrell, Phys. Rev. **135**, A550 (1964).

[4] A. I. Larkin and Yu. N. Ovchinnikov, Zh. Eksp. Teor. Fiz. **47**, 1136 (1964) [Sov. Phys. JETP **20**, 762 (1965)].

[5] G. Sarma, J. Phys. Chem. Solids **24**, 1029 (1963).

[6] W. V. Liu and F. Wilczek, Phys. Rev. Lett. **90**, 047002 (2003).

[7] M. W. Zwierlein *et al.*, Science **311**, 492 (2006); M. W. Zwierlein *et al.*, Nature (London) **442**, 54 (2006); Y. Shin *et al.*, Phys. Rev. Lett. **97**, 030401 (2006); Y. Shin *et al.*, Nature (London) **451**, 689 (2008); G. B. Partridge *et al.*, Science **311**, 503 (2006); G. B. Partridge *et al.*, Phys. Rev. Lett. **97**, 190407 (2006).

[8] T. Mizushima *et al.*, Phys. Rev. Lett. **94**, 060404 (2005); D. E. Sheehy and L. Radzihovsky, *ibid.* **96**, 060401 (2006); J. Kinnunen *et al.*, *ibid.* **96**, 110403 (2006); K. Machida *et al.*, *ibid.* **97**, 120407 (2006); P. Castorina *et al.*, Phys. Rev. A **72**, 025601 (2005); N. Yoshida and S.-K. Yip, *ibid.* **75**, 063601 (2007); W. Zhang and L.-M. Duan, *ibid.* **76**, 042710 (2007); T. K. Koponen *et al.*, New J. Phys. **10**, 045014 (2008).

[9] K. B. Gubbels *et al.*, Phys. Rev. Lett. **97**, 210402 (2006); T. L. Dao *et al.*, *ibid.* **101**, 236405 (2008); C. C. Chien *et al.*, *ibid.* **97**, 090402 (2006); **98**, 110404 (2007).

[10] K. Yang, Phys. Rev. B **63**, 140511(R) (2001); E. Zhao and W. V. Liu, Phys. Rev. A **78**, 063605 (2008); M. M. Parish *et al.*, Phys. Rev. Lett. **99**, 250403 (2007); H. Hu *et al.*, *ibid.* **98**, 070403 (2007); G. Orso, *ibid.* **98**, 070402 (2007).

[11] A. E. Feiguin and F. Heidrich-Meisner, Phys. Rev. B **76**, 220508(R) (2007); M. Tezuka and M. Ueda, Phys. Rev. Lett. **100**, 110403 (2008); M. Rizzi *et al.*, Phys. Rev. B **77**, 245105 (2008); G. G. Batrouni *et al.*, Phys. Rev. Lett. **100**, 116405 (2008); A. Luscher *et al.*, Phys. Rev. A **78**, 013637 (2008); A. Feiguin and H. A. David, Phys. Rev. B **79**, 100507(R) (2009); A. Feiguin and F. Heidrich-Meisner, Phys. Rev. Lett. **102**, 076403 (2009).

[12] M. A. Cazalilla *et al.*, Phys. Rev. Lett. **95**, 226402 (2005).

[13] S. J. Gu *et al.*, Phys. Rev. B **76**, 125107 (2007).

[14] D. S. Petrov *et al.*, J. Phys. B **38**, S645 (2005); M. Iskin and C. A. R. Sá de Melo, Phys. Rev. Lett. **97**, 100404 (2006); G. Orso *et al.*, Phys. Rev. A **77**, 033611 (2008); D. S. Petrov *et al.*, Phys. Rev. Lett. **99**, 130407 (2007); M. M. Parish *et al.*, *ibid.* **98**, 160402 (2007); S. A. Silotri, *et al.*, Eur. Phys. J. D **49**, 383 (2008); G. D. Lin *et al.*, Phys. Rev. A **74**, 031604(R) (2006).

[15] Recently, Batrouni *et al.*, e-print arXiv:0809.4549, used the quantum Monte Carlo technique to study possible phases of the mass imbalanced cold atom Fermi mixture systems. The numerical demand of the QMC technique does not allow for the full mapping of the quantum phase diagram which is our main focus. The two works agree where they overlap.

[16] W. V. Liu *et al.*, Phys. Rev. A **70**, 033603 (2004).

[17] G. Vidal, Phys. Rev. Lett. **91**, 147902 (2003); Phys. Rev. Lett. **93**, 040502 (2004); **98**, 070201 (2007).

[18] E. Wille *et al.*, Phys. Rev. Lett. **100**, 053201 (2008); A.-C. Voigt *et al.*, *ibid.* **102**, 020405 (2009).

[19] E. Altman *et al.*, Phys. Rev. A **70**, 013603 (2004).

[20] L.-M. Duan, Phys. Rev. Lett. **96**, 103201 (2006).